Journal Pre-proof

Effect of the C/N ratio modification on the corrosion behavior and performance of carbonitride coatings prepared by cathodic arc deposition

M.N. Mirzayev, K.M. Hasanov, A.C. Parau, E. Demir, A.S. Abiyev, Tamer Karaman, S.H. Jabarov, M. Dinu, E.P. Popov, A. Vladescu (Dragomir)

Please cite this article as: Mirzayev MN, Hasanov KM, Parau AC, Demir E, Abiyev AS, Karaman T, Jabarov SH, Dinu M, Popov EP, Vladescu (Dragomir) A, Effect of the C/N ratio modification on the corrosion behavior and performance of carbonitride coatings prepared by cathodic arc deposition, *Journal of Materials Research and Technology*, https://doi.org/10.1016/j.jmrt.2023.09.318.

This is a PDF file of an article that has undergone enhancements after acceptance, such as the addition of a cover page and metadata, and formatting for readability, but it is not yet the definitive version of record. This version will undergo additional copyediting, typesetting and review before it is published in its final form, but we are providing this version to give early visibility of the article. Please note that, during the production process, errors may be discovered which could affect the content, and all legal disclaimers that apply to the journal pertain.

Effect of the C/N ratio modification on the corrosion behavior and performance of carbonitride coatings prepared by cathodic arc deposition

M.N. Mirzayev[a,b,c], K.M. Hasanov[a], A.C. Parau[d], E. Demir[e], A.S. Abiyev[f], Tamer Karaman[g], S.H. Jabarov[a], M. Dinu[d], E.P. Popov[h,i], A. Vladescu (Dragomir)[d,j, *]

[a]*Institute of Radiation Problems, Ministry of Science and Education Republic of Azerbaijan, Baku, AZ1143, Azerbaijan*

[b]*Scientific-Research Institute Geotecnological Problems of Oil, Gas and Chemistry, Azerbaijan State Oil and Industry University, AZ1010 Baku, Azerbaijan*

[c]*Western Caspian University, AZ1001 Baku, Azerbaijan*

[d]*National Institute of Research and Development for Optoelectronics INOE 2000, 409 Atomistilor St., 77125, Magurele, Romania*

[e]*Yeditepe University, Faculty of Arts and Sciences, Physics Department, Istanbul, 34755, Turkey*

[f]*Innovation and Digital Development Agency, Baku AZ-1073, Azerbaijan*

[g]*University of Augsburg, Institute of Physics, Physics Department, Augsburg, 86159, Germany*

[h]*Institute for Nuclear Research and Nuclear Energy, Bulgarian Academy of Sciences, Sofia, 1784, Bulgaria*

[i]*Institute of Solid State Physics, Bulgarian Academy of Sciences, Sofia, 1784, Bulgaria*

[j]*Physical Materials Science and Composite Materials Centre, Research School of Chemistry & Applied Biomedical Sciences, National Research Tomsk Polytechnic University, 30 Lenina Avenue, 634050 Tomsk, Russia*

*Corresponding author: alinava@inoe.ro

Abstract: This study focuses on investigating carbonitride coatings, specifically CNTi-(Zr, ZrNb, and ZrSi), as promising candidates for enhancing the durability and efficiency of Ti6Al4V materials used in nuclear fusion technology. X-ray diffraction analysis identified distinct phases, including TiN, ZrN, ZrC, and TiC. The corrosion studies showed complete degradation of the TiN, ZrC, and ZrN phases in the TiZrCN coating after tests, while the TiC phase exhibited relative stability. The surface morphologies and elemental mapping analysis demonstrated the loss of homogeneity in element distribution after corrosion process. The addition of Si and Nb elements into TiZrCN significantly influenced the coatings' corrosion behavior, with breakaway corrosion observed in CNTi- (Zr and ZrSi) coatings and localized corrosion in CNTi-(ZrNb) coatings. Notably, the CNTi-(ZrSi) coating formed an oxide phase in the presence of NaCl, whereas the CNTi-(ZrNb) coating exhibited continuous resistance and a low corrosion rate. Irradiation was carried out for the generation of active isotopes, showing that no radioactive isotopes were formed in any of the investigated samples.

Keywords: Coatings carbonitrides, corrosion, crystal structure, neutron irradiation, surface morphology.

1. Introduction

In recent years, ceramics have gained growing popularity in a range of industrial uses, such as nuclear fusion applications and cutting tools. This surge in interest can be attributed to their remarkable attributes, including exceptional insulation properties, resistance to high temperatures, and resistance to radiation. Notably, ceramics outperform common insulating materials like plastics in these regards. Ceramic materials are highly valuable in various aspects of plasma-facing components, serving as diverters, insulation coatings for coils, and structural components in tokamaks. Because these plasma-facing elements are continually exposed to various types of ionizing radiation originating within the fusion chambers, these materials must possess specific properties that enable them to withstand such conditions effectively. On the other hand, in scenarios where irradiation is only applied during emergencies, the required material properties would differ from those necessary for constant exposure.

In recent years, extensive research efforts have been focused to nitride-based coatings, including but not limited to TiN, ZrN, TiSiN, ZrSiN, ZrTiN, ZrNbN, and ZrTiSiN. These studies have placed a special focus on evaluating their mechanical and elastic properties, residual stress levels, corrosion resistance, and thermal stability [1–8]. Moreover, carbide coatings, including TiC, TiSiC, TiZrC, TiNbC, and TiSiZrC, have exhibited improved tribological performance, due to the inclusion of amorphous carbon (a-C) that acts as a solid lubricant. Additionally, these coatings demonstrate favorable electrical characteristics and resistance to oxidation [9–13]. Notably, studies conducted by Chang et al. have highlighted the significant influence of carbon content on the mechanical and wear properties of TiSiC coatings synthesized through cathodic arc evaporation. Increasing acetylene flow rates lead to reduced friction coefficients [14].

The research field goes further by developing the carbonitride coatings which emerge as a promising solution for protecting components operating in severe corrosion environments, as they combine the desirable characteristics of both nitrides and carbides. The electron concentration and, consequently, specific properties can be tailored for various applications by adjusting the carbon-to-nitrogen (C/N) ratio [15]. For example, TiCN coatings exhibit superior mechanical durability and thermal stability when compared to separate TiC and TiN coatings. This advantage was attributed to the synergistic benefits derived from the incorporation of TiC, which brings increased ductility and an elevated melting point, combined with the enhanced adhesion strength and reduced internal stress resulting from the presence of TiN [18]. Constantin et al. conducted comprehensive investigations into the impact of incorporating small quantities of Zr, Nb, or Si into TiZrCN, TiNbCN, and TiSiCN systems. Their studies revealed a noteworthy reduction in stress and a simultaneous enhancement in adhesion, coupled with significant improvements in the corrosion resistance of high-speed steel when exposed to aggressive NaCl environments [19]. Until now, extensive research efforts have been devoted to the investigation of complex Ti carbonitride coatings prepared using the physical vapor deposition (PVD) methods. These coatings involved the incorporation of alloying elements, such as Cr and/or Si, resulting in the formation of structures such as TiCrCN [20], TiSiCN [21–23], TiCrNbCN [24], TiAlSiCN [25–27], TiCrSiCN [28–30], and TiNbCN [31–33]. Remarkably, carbonitride coatings have demonstrated exceptional properties across a broad range of applications,

2

with TiSiCN coatings being particularly favored for their well-established characteristics, including high hardness, low friction, and excellent wear performance [34]. To date, TiSiCN coatings have been prepared through a range of methods, including magnetron sputtering [22] or chemical vapor deposition (CVD) methods [21, 23, 35]. In a study conducted by Kuptsov et al., the electrochemical behavior of TiCN, TiSiCN, TiCrSiCN, and TiAlSiCN coatings, deposited using reactive DC magnetron sputtering, was compared in 1 N H_2SO_4 and 0.9% NaCl solution. The findings indicated that all the coatings examined exhibited passive behavior in both corrosive environments [16]. Additionally, in a separate study conducted by Caicedo et al., the introduction of Nb into the TiCN matrix within coatings, prepared by magnetron sputtering, led to increased polarization resistance when exposed to a 3.5% NaCl solution [36]. The authors also observed higher impedance semicircles in the Nyquist diagram for the TiNbCN coating when a lower substrate bias was applied. This observation was attributed to increased ion bombardment, leading to a rise in the porosity of the coatings, thus reducing their corrosion resistance. The lower corrosion rate observed for the TiNbCN coating was attributed to the substitution process, where Nb ions replaced Ti ions, leading to the formation of a more stable structure. This substitution resulted in a different energy configuration, with Nb, having a higher electronegativity (1.60) compared to Ti (1.5), ultimately contributing to the enhanced corrosion resistance of the TiNbCN coating [36]. Extensive research has been conducted on other various carbonitride coatings, such as TiCN, TiCrSiCN, TiAlSiCN, TiSiCN, ZrCN, TiNbCN, TiZrCN, TiAlCN, and TiAlZrCN, among others [27, 29, 31].

In previous studies conducted by the authors, stoichiometric quaternary carbonitride coatings (TiZrCN, TiNbCN, TiSiCN) deposited using the cathodic arc technique were thoroughly investigated and compared to TiCN coating in terms of their corrosion resistance in a 3.5% NaCl solution [16]. The results indicated that the TiNbCN and TiZrCN coatings exhibited superior corrosion resistance, highlighting the beneficial effect of Nb as an alloying element. Moreover, the TiSiCN coating demonstrated improved electrochemical behavior, and it was suggested that the presence of amorphous phases such as Si, SiN, and SiCN influenced the corrosion process, as previously demonstrated by Zander et al. [17]. By the present paper, small amount of Si and Nb was added into TiZrCN matrix by forming the quintenary structures in order to find the effect on phase composition and corrosion resistance. The choice of these coatings was made by considering the advantageous impact of adding Si or Nb to TiCN coatings. Furthermore, TiZrCN was specifically chosen due to its demonstrated superior corrosion resistance compared to TiNbCN or TiSiCN coatings. Furthermore, the coatings under study were subjected to irradiation to induce the generation of active isotopes. This step aimed to determine whether these coatings could serve as suitable materials in the fields of nuclear and space technology. Additionally, a thorough examination of the phase and elemental compositions was conducted after the corrosion tests, and the findings were compared with those of a previous study.

When assessing corrosion resistance in harsh environments, the selection of an appropriate testing medium that accurately replicates real-life conditions is of paramount importance. Research has demonstrated that in solutions containing chloride ions, these ions (Cl^-) can penetrate the native oxide layers that form on materials. The protective properties of these layers vary depending on the specific materials in question [34]. Consequently, tailored carbonitride coatings have the potential to effectively block the ingress of Cl^- ions at the interfaces between the coating and the electrolyte,

serving as a corrosion barrier to prevent electrolyte infiltration. When contemplating protective coatings, several factors come into play that can influence corrosion resistance. These factors include the choice of the test solution, distances between the target and substrate, applied target powers, applied substrate bias voltage, ion bombardment, and the composition of the coating [34, 36]. A comprehensive understanding of these factors is essential for the design and optimization of carbonitride coatings for specific applications where corrosion resistance is a critical requirement. Thus, the paper is devoted to evaluate the morphology of coated surfaces after corrosion tests.

2. Experimental details
2.1 Preparation of the coatings

The coatings were prepared using a cathodic arc deposition system. The system utilized different cathodes depending on the desired coatings: a single cathode composed of Ti (85 at.%) and Nb (15 at.%) for TiNbCN; two cathodes, one composed of Ti (85 at.%) and Nb (15 at.%) and the other composed of Zr (99.99% purity) for TiNbZrCN; a single cathode composed of Ti (88 at.%) and Si (12 at.%) for TiSiCN; and twenty-two cathodes made of Zr (99.99% purity) and Ti for TiZrCN. The base pressure of the system was $6.0 \times 10\text{-}4$ Pa. Prior to coating, the samples underwent a pre-biasing step at -1000 V for 10 minutes in an Ar atmosphere at a pressure of 0.2 Pa. The deposition conditions were carefully selected to achieve specific parameters: coatings with Zr, Nb, and Si concentrations ranging from 4 to 12 at. %; a C/N ratio of 0.4 (under stoichiometric) and 1.6 (over stoichiometric); and a (C+N)/(metal+Si) ratio between 0.6 and 0.8. The coatings were labeled as "coating-1" for under-stoichiometric compositions and "coating-2" for over-stoichiometric ones. The gas mass flow rates for coating-1 were set at 25 standard cubic centimeters per minute (sccm) for CH_4 and 65 sccm for N_2, while for coating-2, the gas flow rates were inverted. The arc currents varied, with 90 A for Zr and Ti, and 110 A for TiNb and TiSi. The substrate bias was set at -100 V. These parameters were maintained for a maximum of 40 minutes, resulting in a deposition temperature of 320°C and a coating thickness of approximately 3 μm.

2.2 Experimental Procedures of Neutron Activation Analysis

Neutron Activation Analysis (NAA) is a technique that relies on measuring gamma irradiation intensity resulting from the capture of thermal neutrons by the nuclei of the sample being studied [37]. When thermal neutrons interact with the target nuclei of the sample, excited nuclei (Z, A+1) are formed. In the case of neutron activation analysis using fast neutrons, the nuclei in the sample undergo inelastic collisions, leading to excitation to specific low-lying nuclear levels. Subsequently, these excited levels decay by emitting discrete gamma rays. For this study, neutron activation analysis was conducted at the IBR-2 M pulsed reactor of the Frank Laboratory for Neutron Physics, located at the Joint Institute for Nuclear Research in Dubna, Russia. The reactor offers a fast neutron flux and neutron energies up to E>1 MeV. During irradiation, the nominal power of the reactor was 1450 kW (average power during the cycle period). The reactor cycle started on May 14, 2021, at 20:00, and concluded on May 26, 2021, at 19:00, with a total cycle time of 288 hours. Subsequently, the measurement and analysis of the samples took place on June 2, 2021. The isotope investigated in the spectrum was Co58, with a gamma ray energy of 811 keV, and an effective cross-section value of

0.092 barn was used. Table 1 provides information on the density of fast neutron fluence and irradiation samples.

2.3 Crystal Structure, EDX, and Surface Morphology

The coatings exhibited a thickness of approximately 3 μm. The basic composition of the coatings was investigated using Energy Dispersive X-ray Spectroscopy (EDS). To evaluate the surface morphology of the coatings, Scanning Electron Microscopy (Hitachi 3030PLUS) was employed. The crystal structure, phase composition, texture, and grain size of the coatings were determined through X-ray diffraction (XRD) analysis. A Rigaku SmartLab diffractometer with Cu Kα radiation (wavelength of 1.5405 nm) was utilized in a θ/2θ geometry range of 30-80° with a step size of 0.02°/min, and an incident angle of 3°. Texture and crystallite sizes were calculated based on XRD peak widths using Rietveld analysis.

3. Result and Discussion

3.1 Elemental composition analysis

CNTi coatings, specifically CNTi-(Zr, ZrNb, and ZrSi) coatings, were successfully synthesized on Ti6Al4V substrates. The CNTi coatings were prepared with varying C/N ratios ranging from 1.53 to 1.56 and (C+N)/metal+Si ratios ranging from 0.69 to 0.80, as detailed in Table 2. Analysis of the coatings revealed distinct concentrations of different elements. Among the coatings, the Ti element exhibited the highest concentration, with CNTi-(Zr) coatings containing 40.27% Ti, followed by CNTi-(ZrSi) coatings with 37.63% Ti, and CNTi-(ZrNb) coatings with 34.92% Ti. The C and N elements constituted approximately 29.45% to 30.58% and 18.36% to 19.53% of the coatings, respectively. Additionally, trace amounts of other elements, including Zr, Si, Nb, and Al, were also detected in the coatings.

3.2. Neutron activation of the coatings

In the investigation of material irradiation resistance, it is crucial to quantify the defects created within the crystal structure to understand the impact of ionizing irradiation. In this research, the neutron activation analysis method was employed to measure and reconstruct the neutron spectrum within the irradiation facility. To determine the neutron spectrum, satellite samples containing eight elements and ten isotopes (V, Al, Ti isotopes, Ni, Sn, Au, Co, Na) were utilized. The flux density of fast neutrons was assessed through the activation of nickel to Co-58, as its activity directly correlates with the flux density of fast neutrons. It is noteworthy that nickel exhibits only two neutron capture reactions, resulting in the formation of Co-58. Furthermore, the samples did not show any significant activation after fast neutron irradiation. This finding suggests that the materials under study can be considered radiation-resistant, as they exhibited minimal or no activation under the given irradiation conditions.

3.3. X-ray diffraction analysis

Rietveld analysis, using the diffraction spectrum of the Ti6Al4V substrate shown in Fig. 1, was conducted employing the FULLPROF program package. The crystallographic orientations of the

5

substrate were determined as (100), (002), (102), (110), (103), (112), (201), and (200). All identified peaks align with previously reported results in the literature [38]. Based on experimental observations, the Ti6Al4V substrate exhibits a hexagonal structure with lattice parameters a=b=2.933039 Å and c=4.678893 Å in the P63/mmc phase group (space group). Additionally, minor amounts of free β-Ti in the Im$\bar{3}$m phase group, characterized by a diffraction peak at the (110) orientation at 39.6525°, as well as free Fe in the cubic phase, were detected within the Ti6Al4V substrate [39]. Fig. 2 displays the diffraction spectrum of a TiZrCN sample fabricated on a Ti6Al4V substrate with a C/N ratio of 1.6 (over stoichiometric). Rietveld analysis of the TiZrCN sample revealed the presence of seven distinct phases: TiAlV alpha, TiAlV beta, free Fe in the cubic phase, TiN, ZrN, ZrC, and small quantities of TiC. The lattice parameters of the cubic phase structures (Fm$\bar{3}$m) comprising TiN, ZrN, ZrC, and TiC show a significant resemblance, with values of 4.45108 Å, 4.48536 Å, 4.23194 Å, and 4.19357 Å, respectively. As a result, accurately distinguishing these phases can often be challenging [40-42].

Near the main phase of TiAlV beta, prominent peaks at 2θ values of 34.54°/34.63° and 34.81°/34.9° indicate the presence of characteristic phases of ZrC and ZrN. The broadening of these peaks can be ascribed to the similarities in lattice parameters and ion radii of ZrC and ZrN crystals [43-44]. The occurrence of ZrC and ZrN phases at 40°, 58°, 69°, and 73° in the (200), (220), (311), and (222) crystallographic orientations is attributed to the formation of crystalline structures through chemical reactions involving distinct elemental configurations during the synthesis process. Moreover, the broadening of peaks around 36°-37° in the (111) crystallographic orientation suggests the coexistence of TiC and TiN phases. Furthermore, at 43°, 62°, and 74°, corresponding to the (200), (220), and (311) crystallographic orientations, the presence of peaks associated with TiC and TiN phases, along with an amorphous phase, provides valuable insights into the interrelationship between individual phase conditions. After exposure to corrosion, the TiN, ZrC, and ZrN phases present in the TiZrCN sample undergo complete degradation, as illustrated in Fig.3. The intensity distribution in the diffraction spectrum is significantly influenced by the presence of the substrate. Interestingly, the TiC phase maintains a degree of stability even after undergoing the corrosion process. Fig.4 displays the lattice parameters and unit cell volume of TiZrCN before and after corrosion, which were determined through Rietveld analysis of the stoichiometric sample with a C/N ratio of 1.6. Following corrosion, the ZrC, ZrN, and TiN phases are no longer observable. The changes in lattice parameters observed after corrosion are attributed to the mutual interaction between the sample and the substrate, which results in deformation due to surface stress factors. Specifically, for the TiC phase, the presence of a relatively small surface stress factor contributes to a significant 7.7% increase in the unit cell volume.

Despite the initial identification of TiN, ZrN, ZrC, and TiC as the primary phases in the TiZrCN sample, the introduction of Si induces the formation of new chemical structures within the sample. As a consequence, the TiZrSiCN structure arises, with the presence of Si, Si_3N_4, and ZrO phases observed both before and after corrosion, as depicted in Figs. 5 and 6. The identified phases have been characterized based on their compositions, revealing 15.42% Si, 4.5% Si_3N_4, 13.57% ZrO, and 17.20% ZrC. Furthermore, in the composition, the alpha phase of the Ti6Al4V substrate constitutes 38.21% of the composition, the beta phase accounts for 10.25%, and there is a presence of a free iron phase constituting 2.15%. Comprehensive analyses have also shown an increase in the intensity of the alpha phase of the Ti6Al4V substrate after corrosion. Moreover, the reductions in the

crystallographic orientations of Ti6Al4V beta (200), ZrC (220), ZrO (220), Si (311) and (222), and Si3N4 (422) phases have been observed within the sample. The likelihood of the presence of amorphous carbon, oxide, and nitride phases in the TiZrSiCN sample, with added Si, is significantly diminished.

In Fig.7, the unit cell volume and parameters of the TiZrSiCN sample are presented before and after corrosion, determined through Rietveld analysis of the stoichiometric sample with a C/N ratio of 1.6. The crystal structures of Si, ZrC, Si3N4, and ZrO exhibit cubic symmetry, with ZrC and ZrO corresponding to face-centered cubic (FCC) symmetry, and Si and Si3N4 corresponding to diamond (DIA) symmetry. The TiZrSiCN sample consists of 10.14% Si, 1.25% ZrO, 3.82% ZrC, and 3.25% Si3N4 phases. Despite undergoing minor degradation, the Si, ZrC, Si3N4, and ZrO phases demonstate durability after the corrosion process. A comparative analysis of the experiments reveals that TiZrSiCN samples exhibit superior corrosion resistance in comparison to TiZrCN samples, despite the slight deterioration observed in these phases. To investigate the corrosion properties further, a TiZrNbCN sample was prepared by introducing the Nb element into the TiZrCN base matrix, and its corrosion properties were subsequently investigated. The results, analyzed through Rietveld analysis, reveal the dominant presence of the NbC phase (Figs. 8 and 9), constituting 37.5% of the diffraction spectrum. Additionally, 2.49% corresponds to the Ti6Al4V substrate, TiC, TiN, and ZrC phases. Fig.10 illustrates the lattice parameters and volume of the existing phases in the TiZrNbCN sample before and after corrosion. Rietveld analysis indicates minimal changes in the lattice parameters of the NbC phase, suggesting that the sample underwent texture relaxation. When comparing the contributions of the TiC, TiN, and NbC phases with the alpha and beta phases of the Ti6Al4V substrate, it becomes evident that all these phases exhibited similar characteristics or behavior.
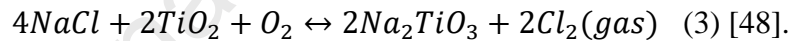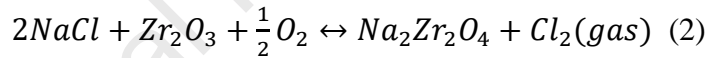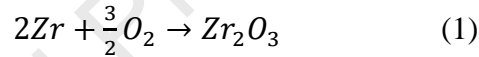
3.3 Surface morphologies and elemental mapping analysis of the of CNTi — (Zr, ZrNb, and ZrSi) samples

The surface of the TiZrCN sample exhibits a homogeneous appearance with the presence of crystalline particles of varying sizes (Fig. 11). The formation of these particles is influenced by two main factors: the synthesis process involving cathodic deposition with different structural combinations, and the presence of surface tensile stress [45-46]. Through structural analysis, it is observed that before corrosion, the TiZrCN surface is characterized by crystalline particles of TiN, ZrN, ZrC, and TiC in the cubic phase. However, after corrosion, the distribution of large-sized crystals on the surface becomes amorphous, while small-sized crystals persist. Upon conducting a comparative analysis of the structural examinations, it is found that only cubic phase ZrC and TiC remain present on the surface after corrosion. A noteworthy observation following corrosion is the occurrence of a preferential degradation process on the TiZrCN surface. Furthermore, elemental mapping analysis demonstrates homogeneity in Ti, C, N, Al, and V elements. However, in the Zr elemental mapping analysis after corrosion, an inhomogeneous distribution of "dark spots" is observed. These "dark spots" can be attributed to "natural" defect sites formed during the synthesis process.

Fig.12 illustrates the presence of small particle inhomogeneities on the surface of TiZrSiCN prior to corrosion. In contrast to the TiZrCN coating, the TiZrSiCN coating shows a prominent distribution of crystalline particles on the surface. Despite the subtle presence of Si, ZrC, Si3N4, and ZrO phases on the coating's surface before corrosion, these phases persist even after the corrosion

process. The corrosion mechanism in the TiZrSiCN coating predominantly occurs in a direction perpendicular to the surface, leading to the observed circular-shaped corrosion patterns. These patterns can be attributed to specific corrosion mechanisms taking place. The analysis of elemental mapping and degradation mechanism indicates that the deformation of the surface is primarily influenced by the presence of carbon. The distribution of elements such as Ti, Si, N, Al, V, Zr, and O exhibits a loss of homogeneity following corrosion. On the other hand, for TiZrNbCN coatings with the addition of Nb, corrosion mechanisms occur in localized areas, as shown in Fig.13. After corrosion, the surface layer of TiZrNbCN coatings displays a layered degradation pattern.

The disruption of elemental mapping homogeneity is ascribed to the accumulation and redistribution of Zr in specific regions of the surface. The corrosion process is influenced by a multitude of factors, including the dissolution temperature of NaCl salts, oxidation, and electrochemical reactions [47]. Both oxidation and electrochemical reactions play a significant role in accelerating the corrosion process on the coating's surface. The formation of chemically reactive oxide interactions on the coating surface indicates the occurrence of "breakaway corrosion". Upon interaction with NaCl salts, the oxidation reactions take place, leading to the generation of an oxide layer and the release of small quantities of gas products [48-52]. These reactions contribute to the overall corrosion process and can affect the durability and integrity of the coatings. Additionally, the presence of different elements and phases within the coatings influences the corrosion behavior, resulting in the observed layered degradation patterns and localized corrosion mechanisms.

$$2Zr + \frac{3}{2}O_2 \rightarrow Zr_2O_3 \qquad (1)$$

$$2NaCl + Zr_2O_3 + \frac{1}{2}O_2 \leftrightarrow Na_2Zr_2O_4 + Cl_2(gas) \quad (2)$$

$$4NaCl + 2TiO_2 + O_2 \leftrightarrow 2Na_2TiO_3 + 2Cl_2(gas) \quad (3) \text{ [48]}.$$

On the other hand, it is possible for Ti, Zr, Fe, Al, V, Si, and Nb elements to undergo reactions with Cl^- ions.

$$Fe + Cl_2 \rightarrow FeCl_2(gas) \quad (3) \text{ [47]}.$$
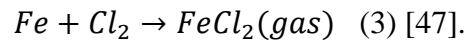
The structural analysis does not indicate the presence of titanium tetrachloride ($TiCl_4$), titanium trichloride ($TiCl_3$), titanium dichloride ($TiCl_2$), zirconocene dichloride ($ZrCl_2$), aluminum chloride ($AlCl_3$), and vanadium chloride (VCl_5) in the dominant phase. Experimental comparisons reveal that exposure to NaCl results in the formation of various corrosion traces on the CNTi-(Zr, ZrNb, and ZrSi) coatings. The addition of Si and Nb elements has a significant influence on the corrosion process. "Breakaway corrosion" is observed on the CNTi-(Zr and ZrSi) coatings, while the CNTi-(ZrNb) surface experiences localized corrosion. Only the CNTi-(ZrSi) coating forms an oxide phase in the presence of NaCl. The CNTi-(Zr) coatings exhibit blistering, a degraded surface, and the formation of recurring and fragmented oxide phases. In comparison, the CNTi-(ZrNb) coating demonstrates continuous resistance, a weak oxidation reaction, and a low corrosion rate when exposed to NaCl.

4. Conclusions

In this work, we successfully synthesized CNTi-(Zr, ZrNb, and ZrSi) coatings on Ti6Al4V substrates with varying C/N and (C+N)/metal+Si ratios. The following conclusions can be drawn:

- Each coating excibited Ti as the most abundant element, and all other as alloying element.

- Both TiZrSiCN and TiZrNbCN coatings demonstrated greater corrosion resistance compared to TiZrCN coatings. The corrosion mechanisms varied among the coatings: TiZrCN coatings exhibited "breakaway corrosion," while the TiZrNbCN coatings experienced localized corrosion. The TiZrSiCN coating displayed a unique corrosion mechanism perpendicular to the surface, resulting in circular-shaped corrosion patterns.
- Neutron activation analysis revealed that the coatings exhibited minimal activation under the given irradiation conditions, indicating their radiation-resistant nature.
- The experiment showed that no radioactive isotopes were formed in any of the bases and samples.

The experimental findings presented in this paper indicated that both TiZrSiCN and TiZrNbCN coatings have the potential to serve as promising materials in the fields of nuclear and space technology.

CRediT authorship contribution statement:

M.N. Mirzayev: Conceptualization, Investigation (neutron activation); Resources, Software, Investigation, Writing - review editing. **K.M. Hasanov:** Investigation. **A. Vladescu (Dragomir)**: Conceptualization, Investigation, Writing - original draft, Writing - review editing, Project administration. **E. Demir:** Investigation (neutron activation); Writing - review editing. **A.C. Parau:** Investigation (SEM analysis). **M.Dinu:** Investigation (corrosion analysis). **A.S. Abiyev:** Investigation (Rievetal analysis, XRD interpretation). **E.P. Popov:** Investigation (Rievetal analysis, XRD interpretation).

Declaration of Competing Interest

The authors affirm that they have no known competing financial interests or personal relationships that could have influenced the work reported in this paper.

References

[1] R. Mareus, C. Mastail, F. Anˇgay, N. Bruneti`ere, G. Abadias, Study of columnar growth, texture development and wettability of reactively sputter-deposited TiN, ZrN and HfN thin films at glancing angle incidence, Surf. Coat. Technol. 399 (2020), https://doi.org/10.1016/j.surfcoat.2020.126130.

[2] P. Yi, L. Zhu, C. Dong, K. Xiao, Corrosion and interfacial contact resistance of 316L stainless steel coated with magnetron sputtered ZrN and TiN in the simulated cathodic environment of a proton-exchange membrane fuel cell, Surf. Coat. Technol. 363 (2019), https://doi.org/10.1016/j.surfcoat.2019.02.027.

[3] Z. Rao, E. Chason, Measurements and modeling of residual stress in sputtered TiN and ZrN: Dependence on growth rate and pressure, Surf. Coat. Technol. 404 (2020), https://doi.org/10.1016/j.surfcoat.2020.126462.

[4] N. Marchin, F. Ashrafizadeh, Effect of carbon addition on tribological performance of TiSiN coatings produced by cathodic arc physical vapour deposition, Surf. Coat. Technol. 407 (2021), https://doi.org/10.1016/j.surfcoat.2020.126781.

[5] Q.L. Tang, Y.C. Wu, B.S. Lou, Z.Y. Chen, J.W. Lee, Mechanical property evaluation of ZrSiN films deposited by a hybrid superimposed high power impulse- medium frequency sputtering and RF sputtering system, Surf. Coat. Technol. 376 (2019), https://doi.org/10.1016/j.surfcoat.2018.03.103.

[6] I.A. Saladukhin, G. Abadias, V.V. Uglov, S.V. Zlotski, A. Michel, A. Janse van Vuuren, Thermal stability and oxidation resistance of ZrSiN nanocomposite and ZrN/SiNx multilayered coatings: A comparative study, Surf. Coat. Technol. 332 (2017), https://doi.org/10.1016/j.surfcoat.2017.08.076.

[7] M.B. Kanoun, S. Goumri-Said, Effect of alloying on elastic properties of ZrN based transition metal nitride alloys, Surf. Coat. Technol. 255 (2014), https://doi.org/ 10.1016/j.surfcoat.2014.03.048.

[8] C.P. Mejía, M.R. Chellali, C.M. Garz´on, J.J. Olaya, H. Hahn, L. Velasco, Effect of discharge current on the corrosion resistance and microstructure of ZrTiSiN coatings deposited by magnetron co-sputtering, Mater. Today Commun. 26 (2021), https://doi.org/10.1016/j.mtcomm.2021.102151.

[9] D.M. Devia, E. Restrepo-Parra, P.J. Arango, Comparative study of titanium carbide and nitride coatings grown by cathodic vacuum arc technique, Appl. Surf. Sci. 258 (2011), https://doi.org/10.1016/j.apsusc.2011.09.061.

[10] A.O. Eriksson, J.Q. Zhu, N. Ghafoor, M.P. Johansson, J. Sj¨olen, J. Jensen, M. Od´en, L. Hultman, J. Ros´en, Layer formation by resputtering in Ti-Si-C hard coatings during large scale cathodic arc deposition, Surf. Coat. Technol. 205 (2011), https://doi.org/10.1016/j.surfcoat.2011.02.007.

[11] A. Pogrebnjak, V. Ivashchenko, O. Maksakova, V. Buranich, P. Konarski, V. Bondariev, P. Zukowski, P. Skrynskyy, A. Sinelnichenko, I. Shelest, N. Erdybaeva, P. Galaszkiewicz, T.N. Koltunowicz, Comparative measurements and analysis of the mechanical and electrical properties of Ti-Zr-C nanocomposite: Role of stoichiometry, Measurement (Lond). 176 (2021), https://doi.org/10.1016/j. measurement.2021.109223.

[12] K.A. Kuptsov, A.N. Sheveyko, O.S. Manakova, D.A. Sidorenko, D.V. Shtansky, Comparative investigation of single-layer and multilayer Nb-doped TiC coatings deposited by pulsed vacuum deposition techniques, Surf. Coat. Technol. 385 (2020), https://doi.org/10.1016/j.surfcoat.2020.125422.

[13] C. Vitelaru, M. Balaceanu, A. Parau, C.R. Luculescu, A. Vladescu, Investigation of nanostructured TiSiC–Zr and TiSiC–Cr hard coatings for industrial applications, Surf. Coat. Technol. 251 (2014) 21–28, https://doi.org/10.1016/j.surfcoat.2014.04.001.

[14] C.L. Chang, Y.W. Chen, Effect of the carbon content on the structure and mechanical properties of Ti-Si-C coatings by cathodic arc evaporation, Surf. Coat. Technol. 205 (2010), https://doi.org/10.1016/j.surfcoat.2010.01.016.

[15] M. Balaceanu, V. Braic, A. Kiss, C.N.N. Zoita, A. Vladescu, M. Braic, I. Tudor, A. Popescu, R. Ripeanu, C. Logofatu, C.C.C. Negrila, Characteristics of arc plasma deposited TiAlZrCN coatings, Surf. Coat. Technol. 202 (2008) 3981–3987, https://doi.org/10.1016/j.surfcoat.2008.02.005.

[16] L. Constantin, M. Braic, M. Dinu, M. Balaceanu, V. Braic, C. Farcau, A. Vladescu, Effects of Zr, Nb, or Si addition on the microstructural, mechanical, and corrosion resistance of TiCN hard coatings, Mater. Corros. (2016) 929–938, https://doi.org/ 10.1002/maco.201508737.

[17] D. Zander, B. Heisterkamp, I. Gallino, Corrosion resistance of Cu-Zr-Al-Y and Zr-

Cu-Ni-Al-Nb bulk metallic glasses, J. Alloy. Compd. 434–435 (2007) 234.

18. Tang, J.-F.; Huang, S.-Y.; Lin, J.-H.; Yang, F.-C.; Chang, C.-L. Mechanical Properties of TiN Deposited in Synchronous Bias Mode through High-Power Impulse Magnetron Sputtering. Surf. Coat. Technol. 2022, 434, 128201.

19. Constantin, L.; Braic, M.; Dinu, M.; Balaceanu, M.; Braic, V.; Farcau, C.; Vladescu, A. Effects of Zr, Nb, or Si Addition on the Microstructural, Mechanical, and Corrosion Resistance of TiCN Hard Coatings. Mater. Corros. 2016, 67, 929–938.

20. He, J.; Nan, Z.; Mi, P.; Chen, K.; Qin, Y. In Situ Nanostructured (TiCr)CN Coating by Reactive Plasma Spraying. Ceram. Int. 2018, 44, 712–717.

21. Ma, S.L.; Ma, D.Y.; Guo, Y.; Xu, B.; Wu, G.Z.; Xu, K.W.; Chu, P.K. Synthesis and Characterization of Super Hard, Self-Lubricating Ti–Si–C–N Nanocomposite Coatings. Acta Mater. 2007, 55, 6350–6355.

22. Xie, X.; Li, J.; Dong, M.; Zhang, H.; Wang, L. Structure and Properties of TiSiCN Coatings with Different Bias Voltages by Arc Ion Plating. Surf. Topogr. 2018, 6, 014003.

23. Wang, H.; Ou, Y.; Zhang, X.; Liao, B.; Ou, X.; Luo, J.; Pang, P.; Chen, L.; Hua, Q.; Bao, M. Tribocorrosion Behaviors of TiSiCN Nanocomposite Coatings Deposited by High Power Impulse Magnetron Sputtering. Mater. Res. Express 2020, 7, 076407.

24. Bondar, O.V.; Postolnyi, B.O.; Kravchenko, Y.A.; Shypylenko, A.P.; Sobol, O.V.; Beresnev, V.M.; Kuzmenko, A.P.; Zukowski, P. Fabrication and Research of Superhard (Zr-Ti-Cr-Nb)N Coatings. Acta Phys. Pol. A 2015, 128, 867–871.

25. Zhang, X.; Li, J.; Xiao, J.; Pi, J.; He, G.; Chen, L.; Zeng, Y.; Jiang, J. Effects of Si Addition on Structure and Mechanical Properties of TiAlSiCN Coatings. Surf. Coat. Technol. 2019, 362, 21–26.

26. Golizadeh, M.; Kuptsov, K.A.; Shvyndina, N.V.; Shtansky, D.V. Multilayer SiBCN/TiAlSiCN and AlOx/TiAlSiCN Coatings with High Thermal Stability and Oxidation Resistance. Surf. Coat. Technol. 2017, 319, 277–285.

27. Shtansky, D.V.; Kuptsov, K.A.; Kiryukhantsev-Korneev, P.V.; Sheveiko, A.N.; Fernandez, A.; Petrzhik, M.I. Comparative Investigation of Al- and Cr-Doped TiSiCN Coatings. Surf. Coat. Technol. 2011, 205, 4640–4648.

28. Li, Q.; Jiang, F.; Leng, Y.; Wei, R.; Huang, N. Microstructure and Tribological Properties of Ti(Cr)SiCN Coating Deposited by Plasma Enhanced Magnetron Sputtering. Vacuum 2013, 89, 168–173.

29. Xin, X.; Tengfei, Z.; Yu, W.; Yan, Y.; Yongxiang, L.; Dong, X.; Nan, H. Microstructure and Mechanical Properties of Ti(Cr)SiC(O)N Coatings Deposited by Plasma Enhanced Magnetron Sputtering. Rare Met. Mater. Eng. 2017, 46, 1762–1767.

30. Chaparro, W.A.; Martin, C.R.; López, E.V. Synergy between Erosion-Corrosion of Steel AISI 4140 Covered by a Multilayer TiCN /TiNbCN, at an Impact Angle of 90◦. Dyna 2013, 80, 101–108.

31. Caicedo, J.C.; Guerrero, A.; Aperador, W. Determination of Multilayer Effect Evidence on Metal Carbon-Nitride System. J. Alloys Compd. 2019, 785, 178–190.

32. Bondarev, A.V.; Kiryukhantsev-Korneev, P.V.; Levashov, E.A.; Shtansky, D.V. Tribological Behavior and Self-Healing Functionality of TiNbCN-Ag Coatings in Wide Temperature Range. Appl. Surf. Sci. 2017, 396, 110–120.

32. Li, W.; Liu, P.; Xue, Z.; Ma, F.; Zhang, K.; Chen, X.; Feng, R.; Liaw, P.K. Microstructures, Mechanical Behavior and Strengthening Mechanism of TiSiCN Nanocomposite Films. Sci. Rep. 2017, 7, 2140.

33. El-Rahman, A.M.A.; Wei, R. A Comparative Study of Conventional Magnetron Sputter Deposited and Plasma Enhanced Magnetron Sputter Deposited Ti–Si–C–N Nanocomposite Coatings. Surf. Coat. Technol. 2014, 241, 74–79.

34. Abraham, S.; Choi, E.Y.; Kang, N.; Kim, K.H. Microstructure and Mechanical Properties of Ti-Si-C-N Films Synthesized by Plasma-Enhanced Chemical Vapor Deposition. Surf. Coat. Technol. 2007, 202, 915–919.

35. K.A. Kuptsov, P.V. Kiryukhantsev-Korneev, A.N. Sheveyko, D.V. Shtansky, Comparative study of electrochemical and impact wear behavior of TiCN, TiSiCN, TiCrSiCN, and TiAlSiCN coatings, Surf. Coat. Technol. 216 (2013) 273–281, https://doi.org/10.1016/j.surfcoat.2012.11.058.

36. J.C. Caicedo, C. Amaya, L. Yate, W. Aperador, Effect of Applied Bias Voltage on Corrosion-Resistance for TiC 1–x N x and Ti 1–x Nb x C 1− y N y Coatings, Appl.Surf. Sci. 256 (2010) 2876.

37. M. Leah, Neutron activation analysis, Encyclopedia of Archaeology, 2008, p.1669-1683

38. I. Halevy, G. Zamir, M. Winterrose, G. Sanjit, Carlos Roberto Grandini, Ariel Moreno-Gobbi, Crystallographic structure of Ti-6Al-4V, Ti-HP and Ti-CP under high-pressure, Journal of Physics: Conference Series 215 (2010) 012013 doi:10.1088/1742-6596/215/1/012013

39. R. Pederson, O. Babushkin, F. Skystedt, R. Warren, 'The Use of High Temperature X-Ray Diffractometry to Study Phase Transitions in Ti6Al-4V', in Titanium Alloys at Elevated Temperature: Structural Development and Service Behaviour, Institute of Materials, ISSN 1336- 5510, London, 2001.

40. Wyckoff, R. W. G. Second edition. Interscience Publishers, New York, New York rocksalt structure Crystal Structures, 1963, 1, 85-237

41. Brager A., An X-ray examination of titanium nitride III, Acta Physicochimica (USSR), 1939, 9, 617-632

42. Minghui Yang; Jennifer A. Rodgers; Lawrence C. Middler; Judith Oró-Solé; A. Belén Jorge; Amparo Fuertes; J. Paul Attfield, Direct Solid-State Synthesis at High Pressures of New Mixed-Metal Oxynitrides: RZrO2N (R = Pr, Nd, and Sm), Inorganic Chemistry, 2009, 48, 11498-11500

43. J. Li, Z. Y. Fu, W. M. Wang, H. Wang, S. H. Lee and K. Niihara: 'Preparation of ZrC by self-propagating high-temperature synthesis, Ceram. Int, 2010, 36, (5), 1681–1686. doi: 10.1016/j.ceramint.2010.03.013

44. M. Pukari and M. Takano: 'Sintering and characterization of ZrN and (Dy,Zr)N as surrogate materials for fast reactor nitride fuel', J. Nucl. Mater, 2014, 444, (1–3), 7–13. doi: 10.1016/j.jnucmat.2013.09.00145.

45. M.N. Mirzayev, A.C. Parau, L.Slavov, M.Dinu, D.Neov, Z.Slavkova, E.P. Popov, M. Belova, K.Hasanov, F.A. Aliyev, A.Vladescu, TiSiCN as Coatings Resistant to Corrosion and Neutron Activation, Materials, 16(5) (2023) p.1835.

46. A. Vladescu, MN Mirzayev, AS Abiyev, AG Asadov, E Demir, KM Hasanov, RS Isayev, AS Doroshkevich, SH Jabarov, Sv Lyubchyk, S Lyubchyk, EP Popov, Effect of Si and Nb additions on carbonitride coatings under proton irradiation: A comprehensive analysis of structural, mechanical, corrosion, and neutron activation properties, Nuclear Materials and Energy, 101457

47 Liu, L., Li, Y. & Wang, F. Corrosion behavior of metals or alloys with a solid NaCl deposit in wet oxygen at medium temperature. Science China Technological Sciences, 55, 369–376 (2012).

48. Shu Y, Wang F, Wu W. Synergistic effect of NaCl and water vapor on the corrosion of 1Cr-11Ni-2W-2Mo-V steel at 500–700°C. Oxidation of Metals, 1999, 51: 97–110

49. Li, R., Liu, L., Cui, Y. Rui Liu, Fuhui Wang. Corrosion behavior of pure Ti under continuous NaCl solution spraying at 600 °C, npj Mater Degrad 6, 53 (2022).

50. A. Buling, J. Zerrer, Increasing the application fields of magnesium by ultraceramic®: Corrosion and wear protection by plasma electrolytical oxidation (PEO) of Mg alloys, Surface and Coatings Technology, 369 (2019) 142-155, doi.org/10.1016/j.surfcoat.2019.04.025.

51. Sankara Narayanan Tsn, Song Park Min Ho Lee, Strategies to improve the corrosion resistance of microarc oxidation (MAO) coated magnesium alloys for degradable implants: Prospects and challenges, Progress in Materials Science 60 (2014) 1-71, doi.org/10.1016/j.pmatsci.2013.08.002.

52. Chang-Yang Li Xiao-Lei Feng Xiao-Li Fan Xiao-Tong Yu Zheng-Zheng Yin M. Bobby Kannan Xiao-Bo Chen Shao-Kang Guan Jun Zhang Rong-Chang Zeng, Corrosion and Wear Resistance of Micro-Arc Oxidation Composite Coatings on Magnesium Alloy AZ31—The Influence of Inclusions of Carbon Spheres, Advanced Engineering Materials, 21 (9) (2019) 1900446, doi.org/10.1002/adem.201900446.

Table 1. Density of flux and fluences of irradiation of the carbon nitride samples for neutron activation analysis

Samples	Density of flux, $n/(cm^2 \times sec)$	Fluence, n/cm^2
TiZr(CN) with Ti_6Al_4V subtract	1.65×10^7	1.71×10^{13}
TiZr(CNSi) with Ti_6Al_4V subtract	1.65×10^7	1.71×10^{13}
TiZr(CNNb) with Ti_6Al_4V subtract	1.65×10^7	1.71×10^{13}

Table 2. Elemental composition of TiZr(CN), TiZr(CNSi) and TiZr(CNNb) samples under different synthesis condition.

Coatings	Ti	Zr	Si	Nb	C	N	O	Al	(C+N)/metal+Si	C/N
TiZr(CN)	40.27	8.72	0	0	29.45	19.13	2.38	0.05	0.71	1.53
TiZr(CNSi)	37.63	8.48	4.29	0	29.11	18.36	2.01	0.12	0.69	1.58
TiZr(CNNb)	34.92	7.81	0	5.06	30.58	19.53	2.01	0.09	0.80	1.56

Table 3. The structure parameters of TiZrCN at C/N of 1.6 over stoichiometric after corrosion and before corrosion.

Crystal structure	Before corrosion			After corrosion		
	Space group	Lattice parameters, Å	Cell volume, Å^3	Space group	Lattice parameters, Å	Cell volume, Å^3
TiAlV alpha	P 63/m m c Hexagonal	a=b=2.93664, c=4.68311	34.97579	P63/mmc Hexagonal	a=b=2.93423, c=4.67889	34.88677
TiAlV beta	Im-3m Cubic	a=b=c=3.21204	33.13929	Im-3m Cubic	a=b=c=3.21978	33.37931
Fe	Fm-3m Cubic	a=b=c=3.58803	46.19226	Fm-3m Cubic	a=b=c=3.58607	46.11662
TiC	Fm-3 m Cubic	a=b=c=4.19357	73.74821	Fm-3 m Cubic	a=b=c=4.29968	79.48923
ZrC	Fm-3 m Cubic	a=b=c=4.45108	88.18512	-	–	–
ZrN	Fm-3 m Cubic	a=b=c=4.48536	90.23881	-	–	–
TiN	Fm-3 m Cubic	a=b=c=4.23194	75.79140	-	-	-

Table 4. The structure parameters of TiZrSiCN at C/N of 1.6 over stoichiometric corrosion before and after corrosion.

Crystal structure	Before corrosion			After corrosion		
	Space group	Lattice parameters, Å	Cell volume, Å³	Space group	Lattice parameters, Å	Cell volume, Å³
TiAlV alpha	P 63/m m c Hexagonal	a=b=2.93196, c=4.67058	34.7311	P63/mmc Hexagonal	a=b=2.93290, c=4.66559	34.75607
TiAlV beta	Im-3m Cubic	a=b=c=3.20465	32.91103	Im-3m Cubic	a=b=c=3.21978	33.37931
Fe	Fm-3m Cubic	a=b=c=3.58506	46.07736	Fm-3m Cubic	a=b=c=3.58279	45.99014
Si	Fd-3m Cubic	a=b=c=5.43070	160.16492	Fm-3 m Cubic	a=b=c=5.43070	160.16492
ZrC	Fm-3 m Cubic	a=b=c=4.38416	84.26738	Fm-3 m Cubic	a=b=c=4.38416	84.26738
Si₃N₄	Fd-3 m Cubic	a=b=c=7.67650	452.36594	Fd-3 m Cubic	a=b=c=7.67650	452.36594
ZrO	Fm-3 m Cubic	a=b=c=4.55264	94.36049	Fm-3 m Cubic	a=b=c=4.55264	94.36049

Table 5. The structure parameters of TiZrNbCN at C/N of 1.6 over stoichiometric before corrosion and after corrosion.

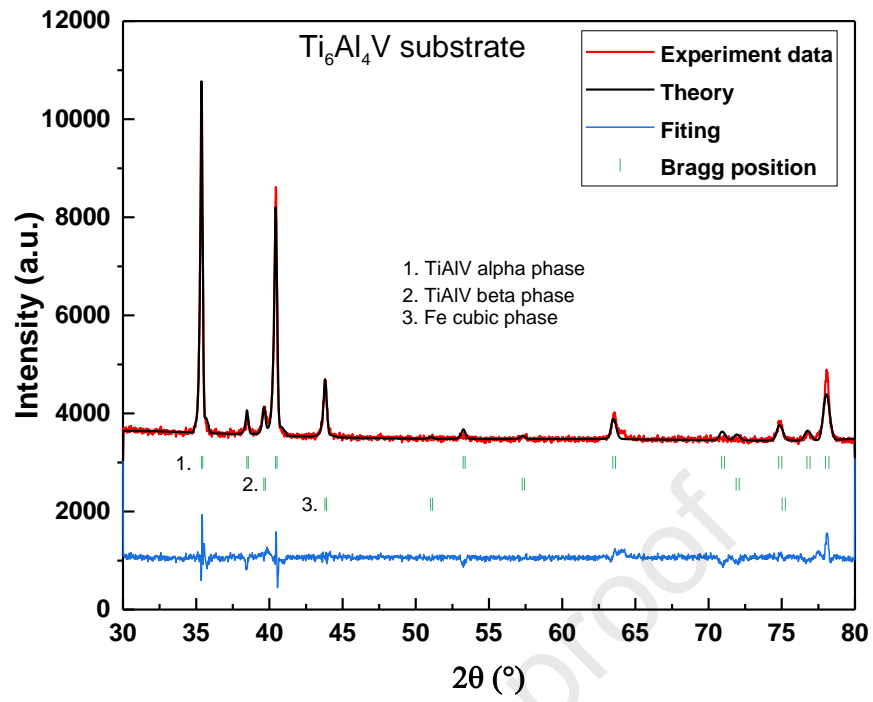| Crystal structure	Before corrosion			After corrosion		
	Space group	Lattice parameters, Å	Cell volume, Å^3	Space group	Lattice parameters, Å	Cell volume, Å^3
TiAlV alpha	P 63/m m c Hexagonal	a=b=2.92793, c=4.66535	34.63665	P63/mmc Hexagonal	a=b=2.92876, c=4.67607	34.73594
TiAlV beta	Im-3m Cubic	a=b=c=3.22233	33.45868	Im-3m Cubic	a=b=c=3.21833	33.33427
Fe	Fm-3m Cubic	a=b=c=3.57858	45.82832	Fm-3m Cubic	a=b=c=3.57858	45.82832
TiC	Fm-3 m Cubic	a=b=c=4.46606	89.07861	Fm-3 m Cubic	a=b=c=4.46606	89.07861
NbC	Fm-3 m Cubic	a=b=c=4.37006	83.45700	Fm-3 m Cubic	a=b=c=4.37006	83.45700
TiN	Fm-3 m Cubic	a=b=c=4.23621	76.02064	Fm-3 m Cubic	a=b=c=4.23621	76.02064
ZrC	Fm-3 m Cubic	a=b=c=4.47055	89.34734	Fm-3 m Cubic	a=b=c=4.47055	89.34734

Figures captions

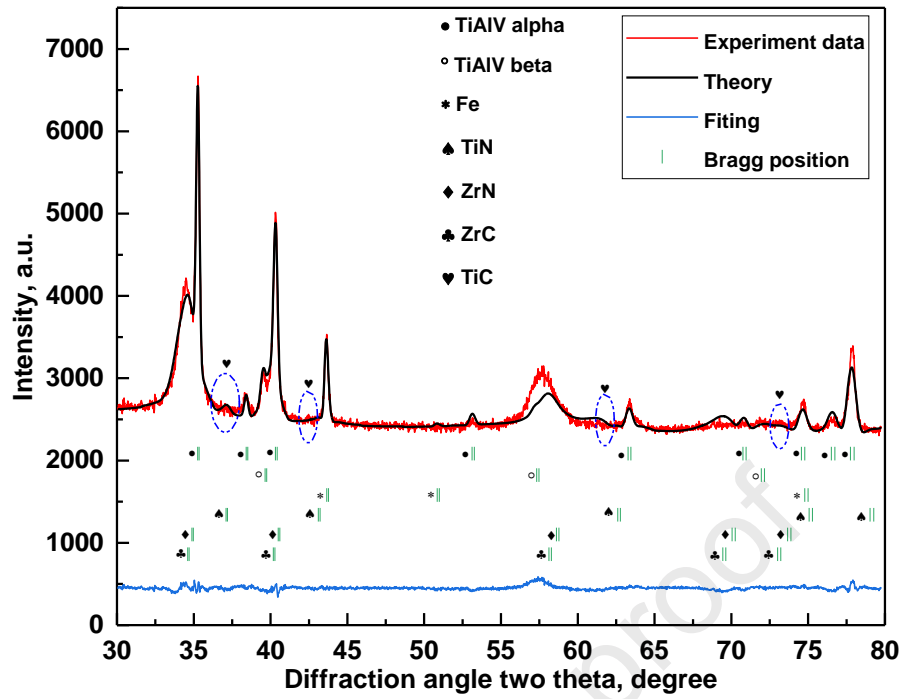Figure 1. X-ray diffraction and Rietveld fit of the Ti-6Al-4V substrate.

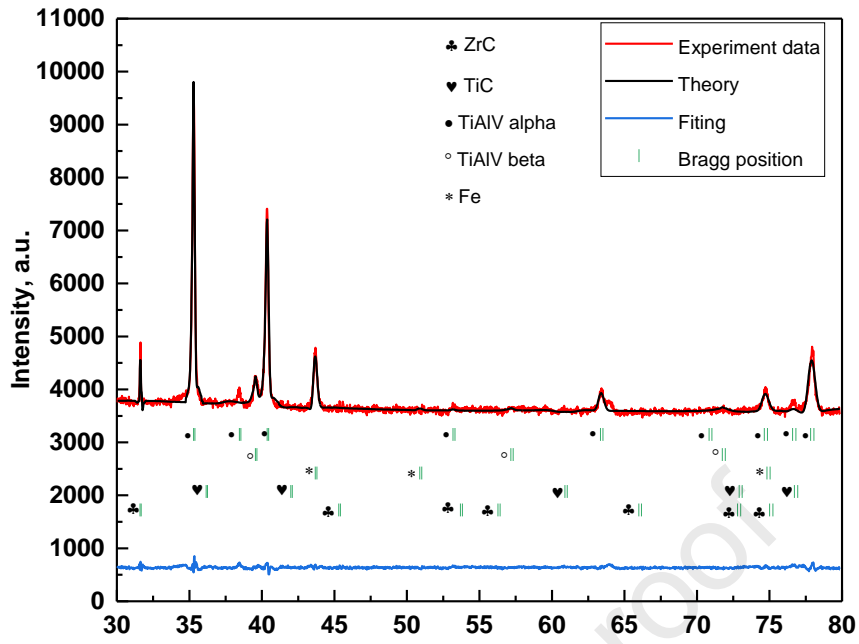Figure 2. The X-ray diffraction pattern of TiZrCN at C/N of 1.6 over stoichiometric before corrosion.

Figure 3. The X-ray diffraction pattern of TiZrCN at C/N of 1.6 over stoichiometric after corrosion.

Figure 4. The structure parameters of TiZrCN at C/N of 1.6 over stoichiometric after corrosion and before corrosion.

Figure 5. The X-ray diffraction pattern of TiZrSiCN at C/N of 1.6 over stoichiometric before corrosion.

Figure 6. The X-ray diffraction pattern of TiZrSiCN at C/N of 1.6 over stoichiometric after corrosion.

Figure 7. The structure parameters of TiZrSiCN at C/N of 1.6 over stoichiometric after corrosion and before corrosion.

Figure 8. The X-ray diffraction pattern of TiZrNbCN at C/N of 1.6 over stoichiometric before corrosion.

Figure 9. The X-ray diffraction pattern of TiZrNbCN at C/N of 1.6 over stoichiometric after corrosion.
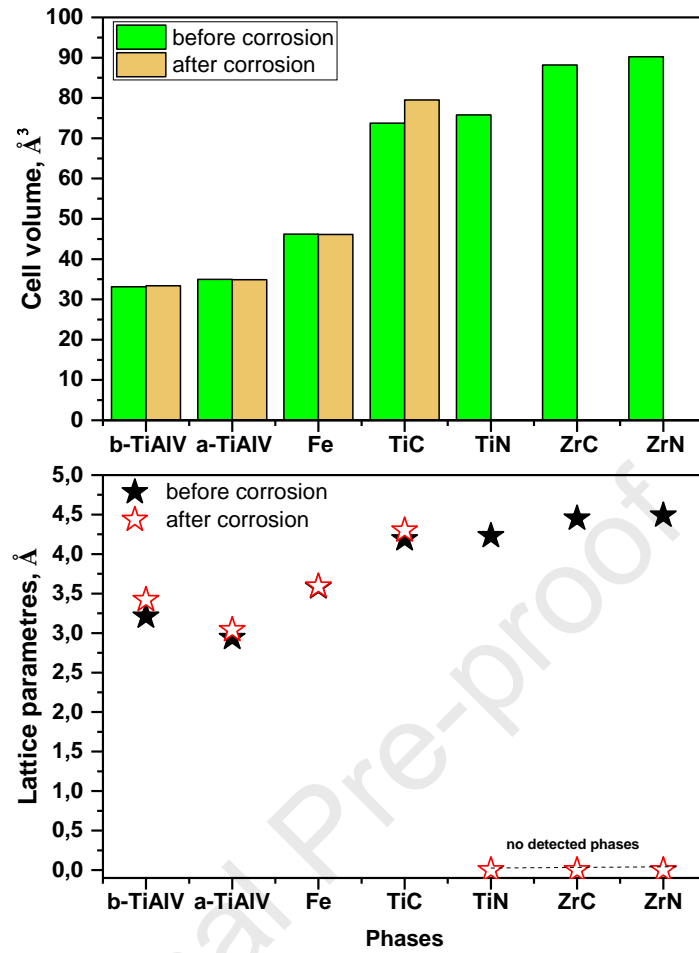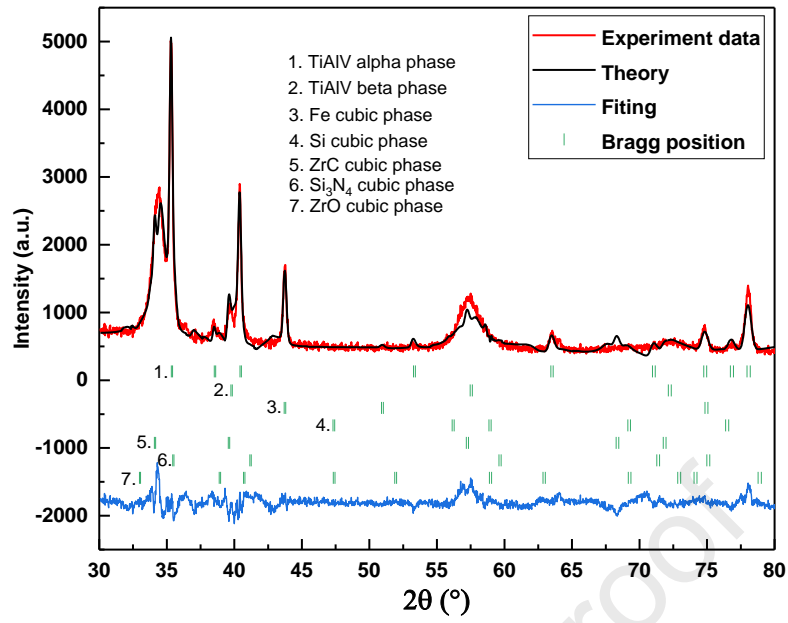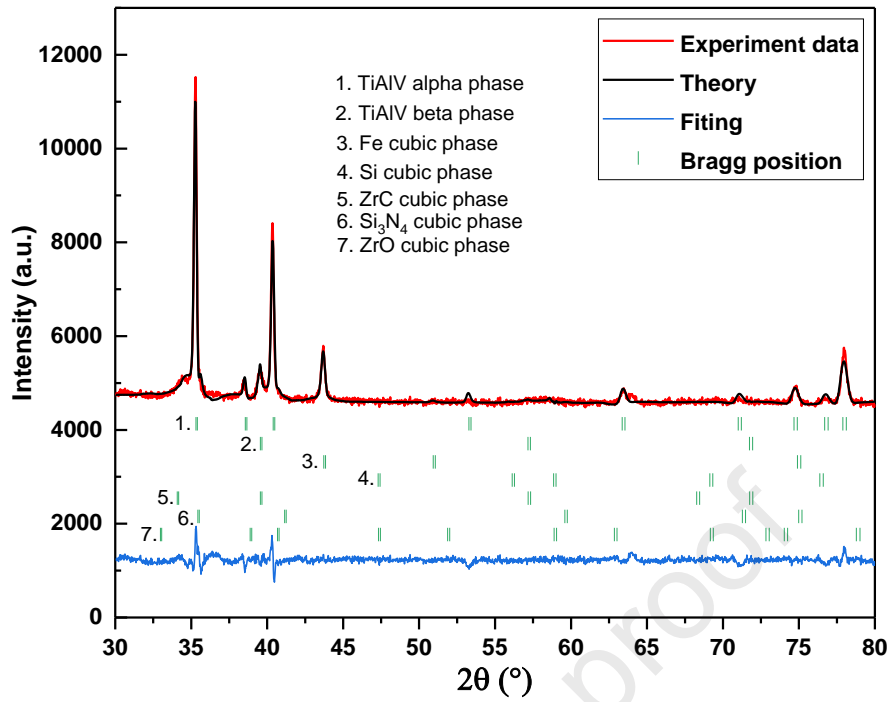
Figure 10. The structure parameters of TiZrNbCN at C/N of 1.6 over stoichiometric before corrosion and after corrosion.

Figure 11. Scanning electron photomicrographs of TiZrCN polished section with Ti6Al4V substrate before corrosion and after corrosion and elemental mapping analysis of TiZrCN before and after corrosion; Showed Ti, C, N, Al, V, Zr and O elements, respectively.

Figure 12. Scanning electron photomicrographs of TiZrSiCN polished section with Ti_6Al_4V substrate before corrosion and after corrosion and elemental mapping analysis of TiZrSiCN before and after corrosion; Showed Ti, Si, C, N, Al, V, Zr and O elements, respectively.

Figure 13. Scanning electron photomicrographs of TiZrNbCN polished section with Ti6Al4V substrate c1) before corrosion and c2) after corrosion and elemental mapping analysis of TiZrNbCN before and after corrosion; Showed Ti, Nb, C, N, Al, V, Zr and O elements, respectively.

Figure 1. X-ray diffraction and Rietveld fit of the Ti-6Al-4V substrate.

Figure 2. The X-ray diffraction pattern of TiZrCN at C/N of 1.6 over stoichiometric before corrosion.

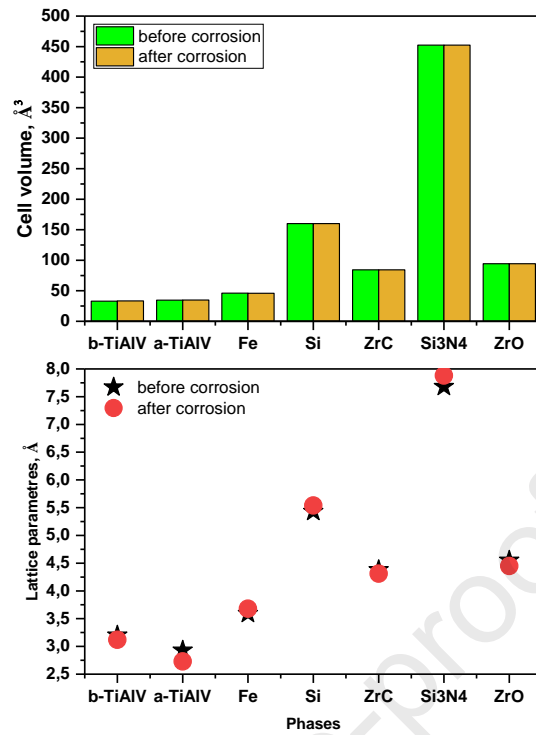Figure 3. The X-ray diffraction pattern of TiZrCN at C/N of 1.6 over stoichiometric after corrosion.

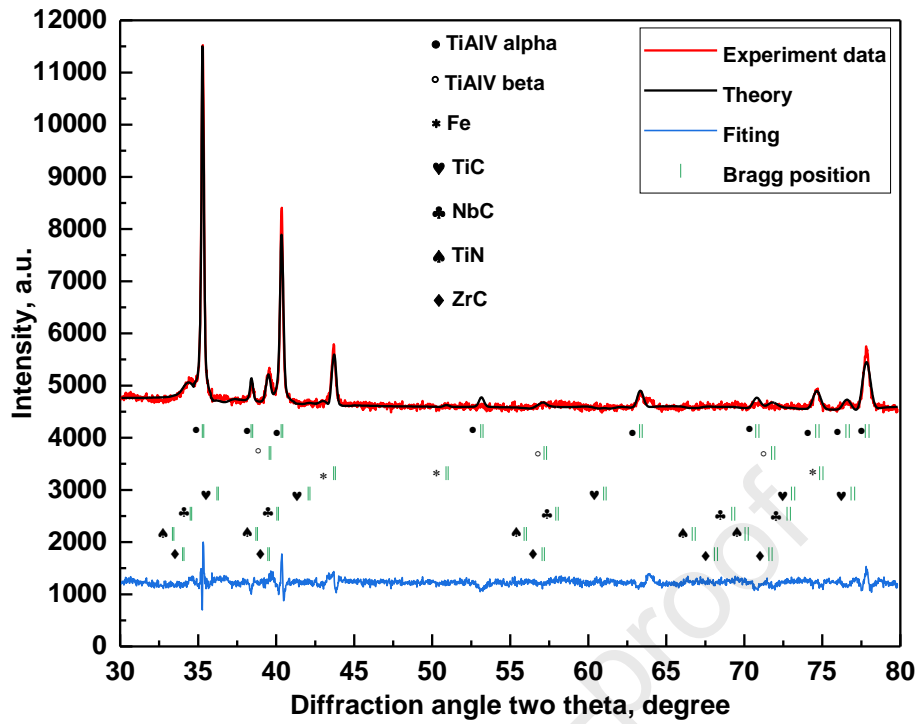Figure 4. The structure parameters of TiZrCN at C/N of 1.6 over stoichiometric after corrosion and before corrosion.

Figure 5. The X-ray diffraction pattern of TiZrSiCN at C/N of 1.6 over stoichiometric before corrosion.
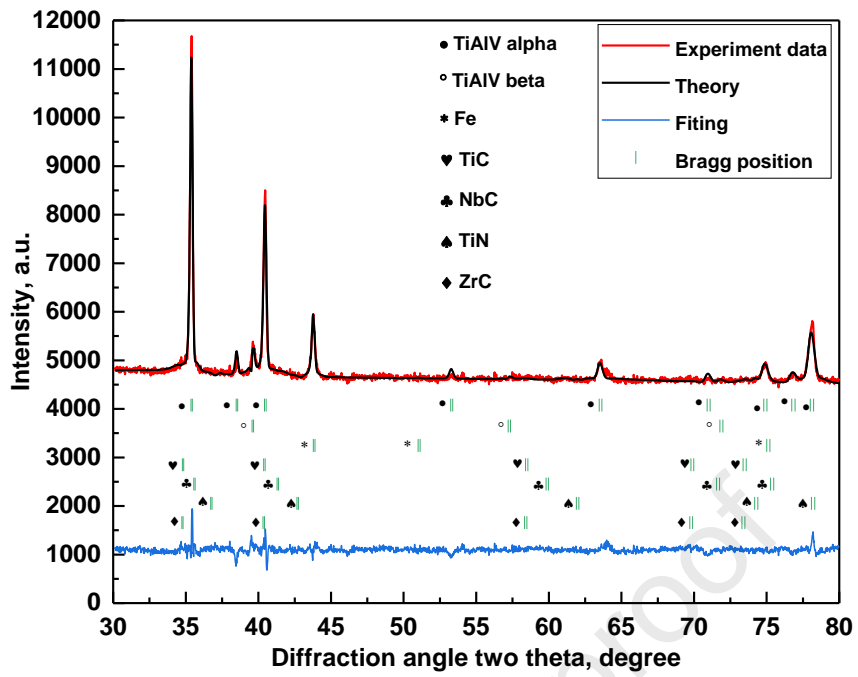
Figure 6. The X-ray diffraction pattern of TiZrSiCN at C/N of 1.6 over stoichiometric after corrosion.
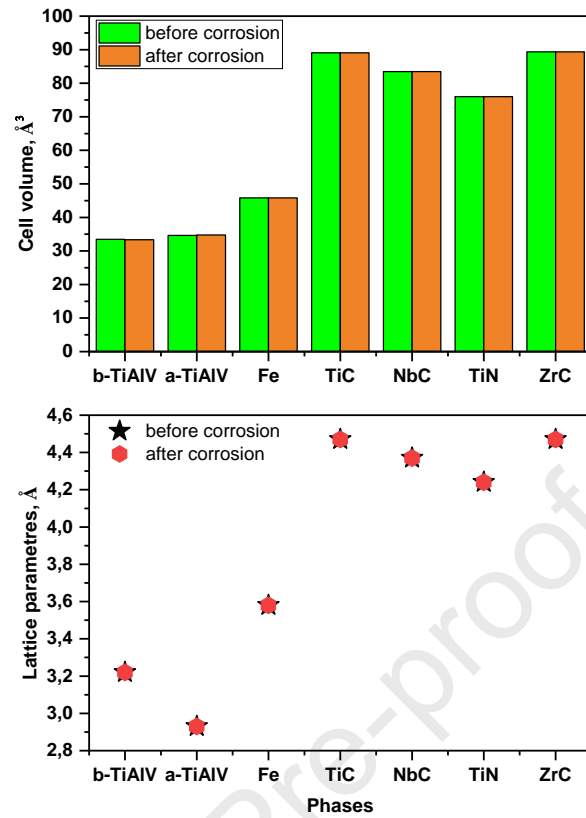
Figure 7. The structure parameters of TiZrSiCN at C/N of 1.6 over stoichiometric after corrosion and before corrosion.

Figure 8. The X-ray diffraction pattern of TiZrNbCN at C/N of 1.6 over stoichiometric before corrosion.

Figure 9. The X-ray diffraction pattern of TiZrNbCN at C/N of 1.6 over stoichiometric after corrosion.

Figure 10. The structure parameters of TiZrNbCN at C/N of 1.6 over stoichiometric before corrosion and after corrosion.
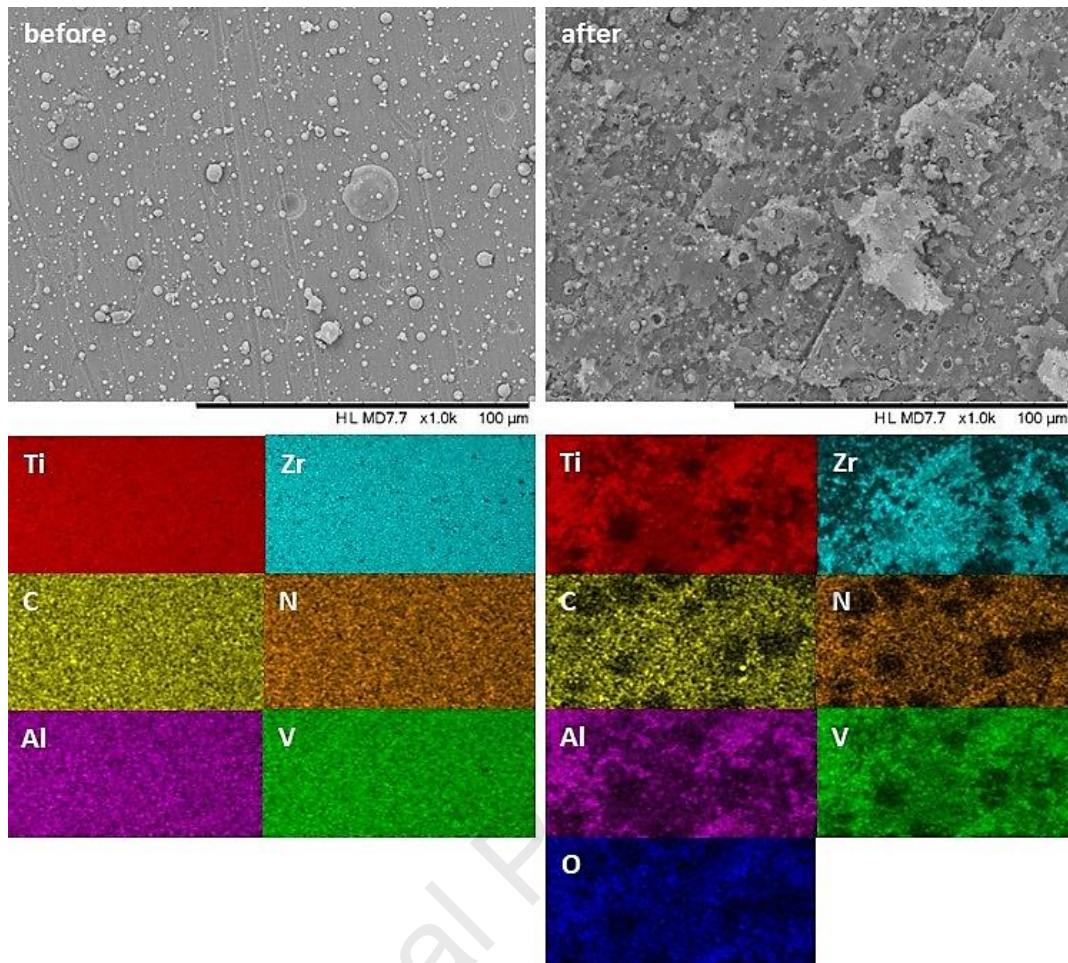
Figure 11. Scanning electron photomicrographs of TiZrCN polished section with Ti6Al4V substrate before corrosion and after corrosion and elemental mapping analysis of TiZrCN before and after corrosion; Showed Ti, C, N, Al, V, Zr and O elements, respectively.
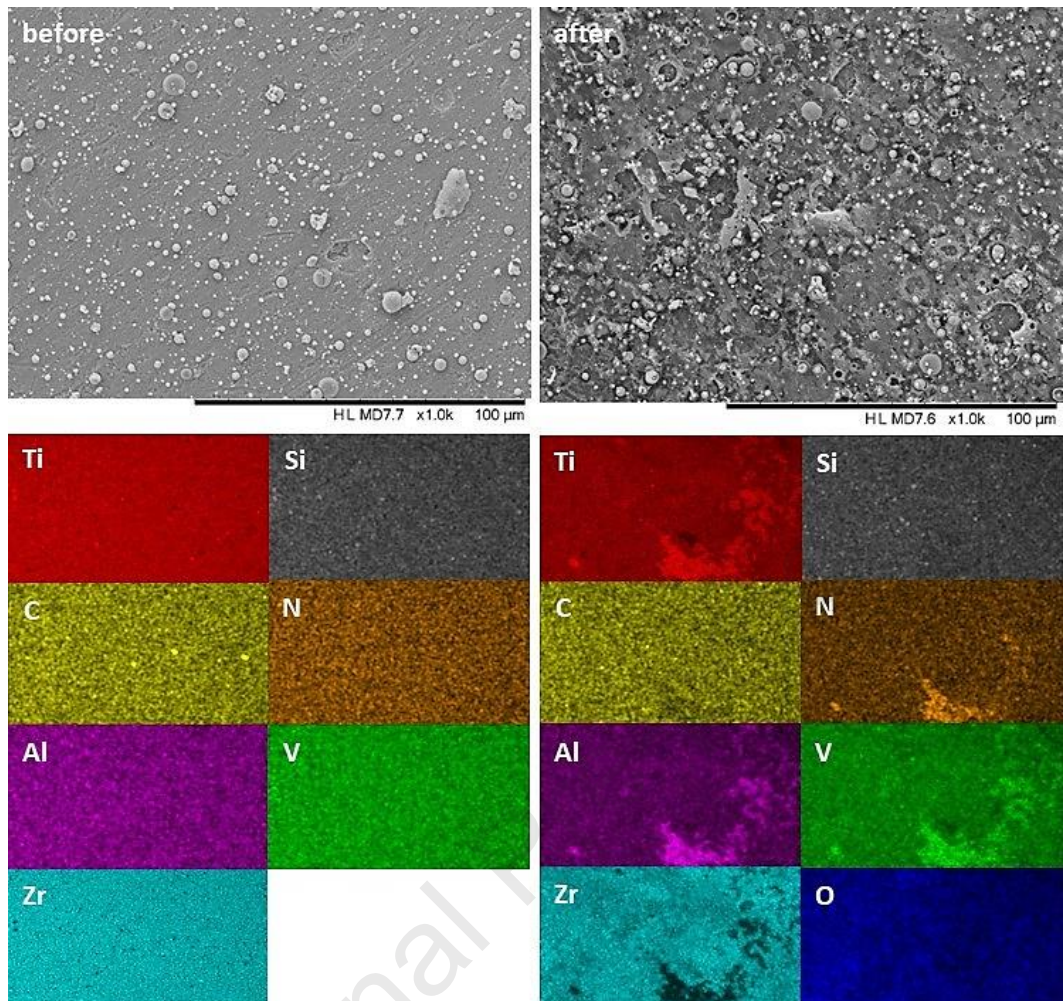
Figure 12. Scanning electron photomicrographs of TiZrSiCN polished section with Ti$_6$Al$_4$V substrate before corrosion and after corrosion and elemental mapping analysis of TiZrSiCN before and after corrosion; Showed Ti, Si, C, N, Al, V, Zr and O elements, respectively.
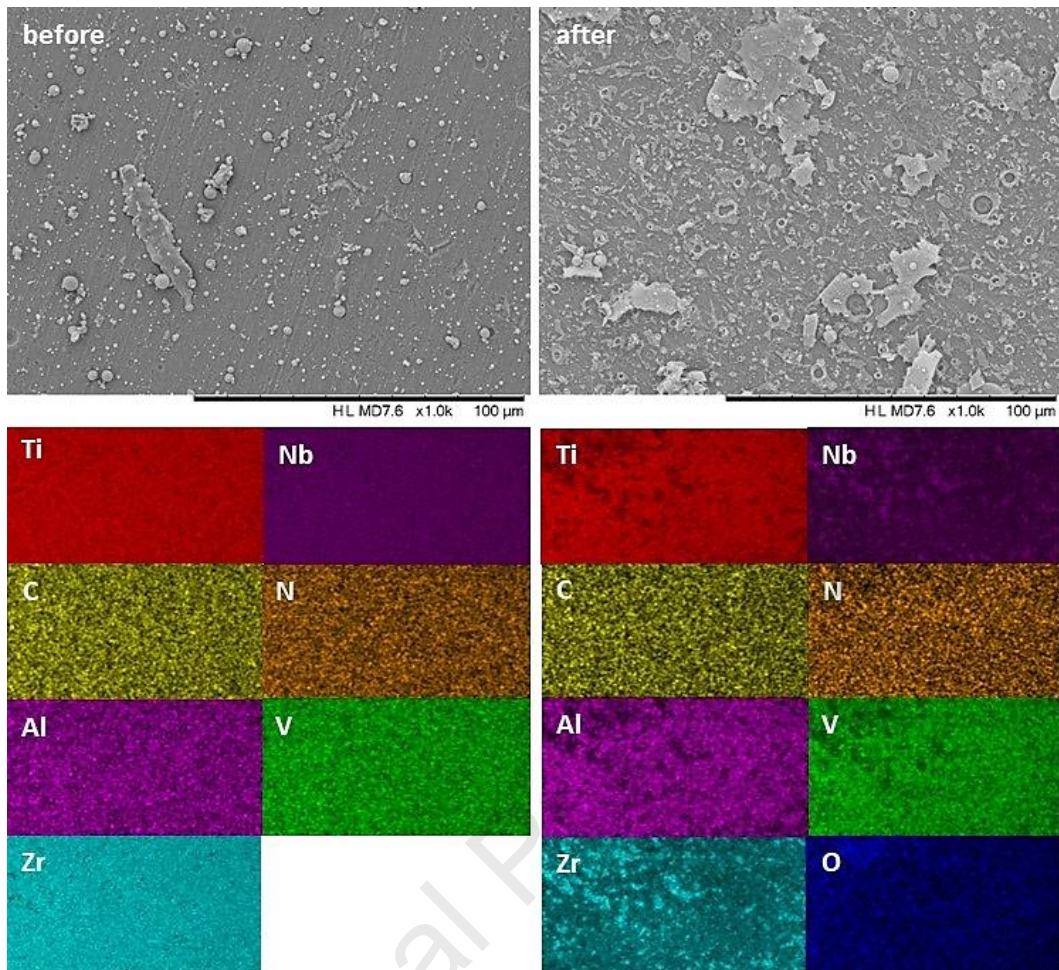
Figure 13. Scanning electron photomicrographs of TiZrNbCN polished section with Ti6Al4V substrate c1) before corrosion and c2) after corrosion and elemental mapping analysis of TiZrNbCN before and after corrosion; Showed Ti, Nb, C, N, Al, V, Zr and O elements, respectively.

Title: "Effect of the C/N ratio modification on corrosion behavior and performance of carbonitride coatings prepared by cathodic arc deposition "

Dear Editor,

I hope this letter finds you well. I am writing to submit our manuscript entitled " Effect of the C/N ratio modification on corrosion behavior and performance of carbonitride coatings prepared by cathodic arc deposition" for consideration for publication in Journal of Materials Research and Technology.

We believe that the insights presented in this manuscript are of significant value to researchers and engineers working in the field of materials science. The findings contribute to tailoring the composition and design of carbonitride coatings to enhance their corrosion resistance and performance in various applications. **We have carefully followed the journal's guidelines for manuscript preparation and have provided the necessary figures and tables to support our findings. No potential conflicts of interest or competing financial interests exist among the authors.**

We kindly request the esteemed editorial board to consider our manuscript for publication in Journal of Materials Research and Technology. **The work has not been submitted elsewhere and has not been previously published. We are confident that our research aligns well with the focus and scope of your esteemed journal.**

Thank you for considering our submission. We look forward to hearing from you and receiving feedback from the reviewers.

Sincerely,

Dr. Eng. Alina Vladescu

National Institute of R&D for Optoelectronics-INOE2000

Department for Advanced Surface Processing and Analysis by Vacuum Technologies - ReCAST
Atomistilor no. 409, P.O.Box MG 05,
Magurele - Bucharest,
077125, ROMANIA
Phone/fax: +4021-457 57 59
web: http://recast.inoe.ro
email: alinava@inoe.ro

orcid: 0000-0001-5770-4541